

Article

Neoproterozoic Lysan Alkaline–Ultramafic Complex in the Eastern Sayan, Southern Siberia, Russia: Mineralogical Constraints of Carbonate Rocks and Albitite for Petrogenesis

Tatiana B. Kolotilina * , Aleksey S. Mekhonoshin  and Yuri D. Shcherbakov

Vinogradov Institute of Geochemistry, Russian Academy of Sciences, Siberian Branch, 1A Favorskogo Str., 664033 Irkutsk, Russia; mekhonos@igc.irk.ru (A.S.M.)

* Correspondence: tak@igc.irk.ru; Tel.: +7-3952424601

Abstract: The Lysan alkaline–ultramafic complex is located in the Sisim shear zone at the contact of the two largest tectonic structures of the accretion–collisional belt in the southwestern frame of the Siberian craton. Intrusions of the complex consist of ore-bearing olivinites, kaersutite clinopyroxenites, and banded kaersutite gabbro, which have been «cut» by albitite dykes and veins. The veins and veinlets of the carbonate rocks are mainly associated with the albitites. The present paper represents the first detailed mineralogical study of carbonate rocks and albitites in the Podlynsky Massif of the Neoproterozoic Lysan alkaline–ultramafic complex. The mineral composition was determined in situ in a polished section by scanning electron microscopy, energy dispersive spectrometry, and electron probe microanalysis. The carbonate rocks of the Podlynsky Massif have been found to contain minerals that are typical of siderite–carbonatites (*sensu stricto*), including calcite, siderite, phengitic muscovite, apatite, monazite, REE fluorocarbonates, pyrite, and sphalerite. These rocks are enriched in light rare earth elements due to the presence of monazite-(Ce), bastnäsite-(Ce), parisite-(Ce), and synchysite-(Ce). The albitites were formed as a result of the fenitization of leucocratic gabbro by alkali-rich carbo-hydrothermal fluids in zones of intense development of tectonic fractures. Infiltration was the dominant mechanism of fenitization. The obtained data significantly enhance the current understanding of the geochemical and ore specialization of rocks in the Lysan Complex.



Citation: Kolotilina, T.B.; Mekhonoshin, A.S.; Shcherbakov, Y.D. Neoproterozoic Lysan Alkaline–Ultramafic Complex in the Eastern Sayan, Southern Siberia, Russia: Mineralogical Constraints of Carbonate Rocks and Albitite for Petrogenesis. *Minerals* **2024**, *14*, 290. <https://doi.org/10.3390/min14030290>

Academic Editor: Federica Zaccarini

Received: 7 February 2024

Revised: 6 March 2024

Accepted: 7 March 2024

Published: 10 March 2024



Copyright: © 2024 by the authors. Licensee MDPI, Basel, Switzerland. This article is an open access article distributed under the terms and conditions of the Creative Commons Attribution (CC BY) license (<https://creativecommons.org/licenses/by/4.0/>).

Keywords: calcite–siderite carbothermalites; sodic metasomatism; fenites; monazite-(Ce); REE fluorocarbonates

1. Introduction

Carbonatites are defined as magmatic rocks in which the modal amount of primary carbonate minerals exceeds 50% [1]; however, they are, in fact, extremely diverse rocks. In general, they can be categorized into two groups: primary carbonatites and carbothermal residues [2,3]. Primary carbonatites can be further subdivided into those associated with the eruption of nephelinites, melilitites, kimberlites, and specific mantle silicate magmas formed by partial melting [2,4]. Meanwhile, carbothermal residues are generated by low-temperature fluids rich in CO₂, H₂O, and fluorine [2,4]. The geochemical characteristics of each genetic type of carbonatite are different [3,5–7]. In addition, carbonatites and carbothermal residues exhibit unique and diverse mineralization with associated mineral assemblages including Fe, P, Ba, Sr, high field strength (Nb, Zr, Ti), and rare earth elements (REEs). As such, carbonatite massifs are a critical source of numerous mineral deposits [7–10].

The dominant rock-forming minerals in carbonatites are calcite, dolomite, and ankerite. Compared to other rock types, magnesite- and siderite-rich carbonatites are less abundant. The position of REE-rich siderite carbonatites (*sensu lato*) in the overall sequence of carbonatite formation processes remains unclear and is of significant interest to researchers [11–16].

Crystallization and cooling of carbonatite and alkaline–ultrabasic melts are accompanied by processes of metasomatic transformation of rocks. Fenites are formed as a result

of these processes [5,17–22]. The study of fenites has been ongoing for over 100 years. Even prior to the introduction of the term “fenite” into scientific use [23], these geological formations have attracted the attention of numerous geologists. Interest in fenites has remained constant over a long period of time [24,25]. The investigation of fenites is crucial for reconstructing the composition of metasomatizing fluids and, ultimately, the original magma [5,17–25]. The mineral composition of fenites is variable and is influenced by several factors, such as the composition, permeability, and structure of the protolith, fluid composition, temperature, and pressure [5,19,20].

The Neoproterozoic Lysan alkaline–ultramafic complex massifs are situated in the Sisim shear zone, at the intersection of two major tectonic structures of the accretion–collisional belt in the southwestern region of the Siberian Craton. Their formation has been a subject of debate for a significant period [26,27]. Recent geochemical and mineralogical discoveries have made it possible to classify these rocks as alkaline–ultramafic complex formations [28]. This hypothesis is supported by the discovery of carbonate rocks with REE mineralization in an albitite “dyke”. These “dykes” are found in crushing zones at contacts between petrographic rock differences within the massifs of the Lysan Complex or at contacts with host rocks. It was previously believed that these dykes were of magmatic origin [26].

This work presents the first data on the chemical composition of the mineral phases of carbonate rocks and albitites from the Podlysan Massif of the Lysan Complex. The sequence of mineral formation has been established. Furthermore, a novel comprehension of the origins of albitites is put forward.

2. Geological Background

2.1. Summary of Geological Features of Neoproterozoic Alkaline Carbonatite Complexes

2.1.1. South Siberia

In the Neoproterozoic period (670–630 Ma), there was widespread intraplate magmatic activity along the western, southwestern, and southeastern (in modern coordinates) margins of the Siberian craton [29–31]. This phenomenon resulted in the formation of several alkaline complexes with carbonatites (Figure 1) [29,32–48]. The Lysan Complex intrusions were also formed during this period [28].

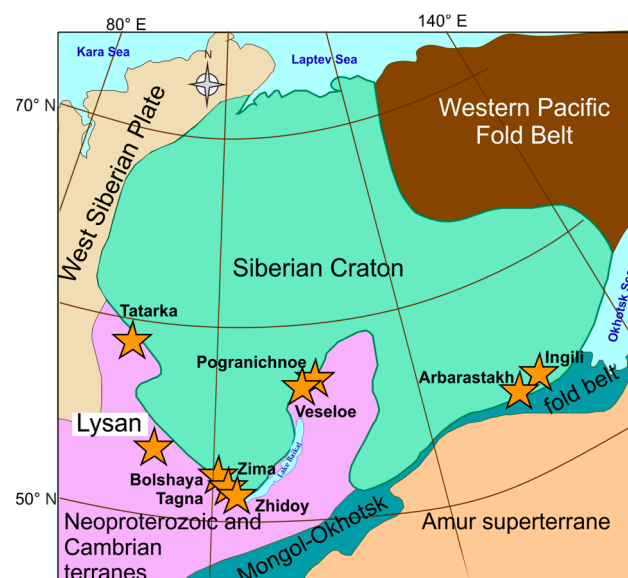


Figure 1. Location of Neoproterozoic alkaline–ultramafic complexes with carbonatites (orange star) in South Siberia. The data used to create this map are sourced from [49].

Neoproterozoic alkaline–carbonatite complexes in southern Siberia are located in the Yenisei Ridge, East Sayan, North Baikal region, and Eastern Aldan. The alkaline igneous complexes in the Yenisei Ridge are located within the Tatarka–Ishimbinskaya suture zone

of the Neoproterozoic accretionary–collisional structure on the southwestern margin of the Siberian craton. These are small plutons within the Tatarka Complex [32,33]. The East Sayan alkaline carbonatite massifs are situated within the Early Proterozoic Urik-Iya graben and the Late Archean Zhidoy Block of the Sharyzhalgai basement uplift of the Siberian craton [34–38]. The Urik-Iya graben is located in the southern part of the Siberian craton, between the Sharyzhalgai and Biryusinsk basement uplifts. It is a linear zone that extends in the northwest direction. The Bolshaya Tagna, Belaya, and Srednaya Zima Complexes are located in the Urik-Ya graben, while the Zhidoy Massif is situated in the basement uplift [39–41]. The carbonatites in the North Baikal region, specifically Pogranichnoye and Veseloye, are located in the eastern part of the Neoproterozoic Baikal-Muya fold belt, adjacent to the North Muya Block [42,43]. The Arbarastakh and Ingili alkaline–ultramafic complexes are located in the eastern part of the Archean Aldan Shield [44–48].

The massifs of the Tatarka Complex (Srednetatarka and Yagodka) are composed of feldspar ijolites with tributaries of urtites and of alkaline syenites and dominant nepheline syenites [32,33]. There are various types of pegmatite and post-magmatic altered rocks that have undergone hydrothermal alteration by microclinization and albitization [33]. The Penchenga carbonatite complex is located 80 km to the northeast of the Srednetatarka Massif [32,33,50]. The carbonatites in this complex form dykes up to 200 m wide and 3 km long. They vary in composition and are represented by calcite, dolomite–calcite, and ankerite–calcite carbonatites [32,33,50].

The Bolshaya Tagna, Belaya and Srednaya Zima are multiphase intrusions [34–37]. This is a series of massifs at varying levels of erosion. They are thought to be branches of a single-ore magmatic system [34]. The following sequence of rock formation is observed: melteigites → ijolites → nepheline syenites → calcite carbonatites → calcite–dolomite carbonatites → ankerite carbonatites. The syenites are cut by dykes of porphyritic picrite, alnoite, damkjernite, and aillikite [36].

The Zhidoy Massif is composed of perovskite and ilmenite pyroxenites [39–41]. Some researchers have identified up to four varieties of pyroxenite in the massif [41]. Ijolites and melteigites form dykes. Carbonatites are found in veins 0.2–5 m thick. They are calcite carbonatites with biotite, apatite, sulphides, REE carbonate, and fluorocarbonate [39].

The Pogranichnoye and the Veseloye are complexes of dolomitic carbonatite dykes with minor amounts of calcite [42,43]. No comagmatic silicate alkaline rocks were discovered associated with carbonatites [43].

The Arbarastakh Massif has a concentric shape [44,50]. The main phase is pyroxenite [44] or, as these rocks are now classified, jacupirangite [45]. Bodies of phoscorite exist in the centre of the complex [44,46]. Numerous arcuate carbonatite sheets are concentrically arranged within the jacupirangite. Ultrabasic lamprophyre dykes are also present [45]. Carbonatites are represented by a number of varieties. These include silicocarbonatites, calcite, calcite–dolomite, dolomite and ankerite carbonatites. About 90% of the carbonatites in the complex are calcite and calcite–dolomite carbonatites [50].

The Ingili Massif occurs as a concentrically zoned body. Its core consists of ijolite, melteigite and urtite. It is surrounded by dykes, stocks, and veins of leucocratic nepheline gabbro, theralites, nepheline syenites, nepheline pyroxenites, nepheline–amphibole rocks, and carbonatites [48,50]. Two generations of carbonatites are distinguished. The first generation is represented by biotite and amphibole–biotite calcite carbonatites [48]. Carbonatites of the second generation are calcite and dolomite–calcite [48].

Thus, most of the Neoproterozoic alkaline complexes with carbonatites in South Siberia belong to central-type alkaline–ultramafic complexes. Only the complexes of the Yenisei Ridge belong to the linear fracture-type complexes. Carbonatites in alkaline–ultramafic complexes of the linear fracture type are typically restricted to lower-order fault systems, in contrast to those of the central-type complexes. The Lysan complex massifs are characterized by zonal rock assemblages and shear zone-type tectonic positions [51].

2.1.2. North America and Baltic Region

Neoproterozoic alkaline complexes with carbonatites are considered to be significant indicators of the breakup zone of Laurasia into the Siberian and Laurentian continents [29]. They can be traced on both sides of this boundary. In North America and the Baltic region, they are found along the rifted margin of the Laurentian crystalline basement [52–55] and the pre-Caledonian margin of the Baltica [52,56].

The Tornat Mountains, Aillik Bay, Baie-Des-Moutons (Mutton Bay), Quigussaq (Umanak), Holsteinsborg, and Sarfartoq complexes are located in the Labrador Sea region of North America, including the Canadian and West Greenland sides. In all complexes, except Baie-Des-Moutons and Sarfartoq, carbonatites are associated with ultramafic lamprophyres [52–55]. The Baie-des-Moutons intrusion is a ring complex composed mainly of syenite [53]. Syenites are cut by small dykes of calcite carbonatites and carbonate-rich lamprophyres. The Sarfartoq carbonatite complex consists of a 15 km² core of carbonatites and fenites, surrounded by an extensive marginal zone that contains carbonatite dykes. Carbonatites are dolomitic and calcitic [53].

There are two well-studied alkaline complexes with carbonatites in the Baltic region: Alnö and Fen [52,56]. The Alnö igneous complex comprises alkaline silicate rocks such as ijolite, nepheline–syenite, and pyroxenite, as well as calcite and silico-calcite carbonatites. These rocks are arranged in a semi-circular pattern [57].

The Fen Complex is considered one of the world's classic carbonatite complexes. It was at this location that the igneous nature of carbonatite was initially recognized. The Fen Complex is a diatreme intrusion composed of carbonatite, ijolite, and pyroxenite [53]. Carbonatites are calcite–dolomite. Fenitization zones are widely developed around the carbonatite dykes and alkaline intrusions.

Comparing the Neoproterozoic alkaline complexes of southern Siberia, North America, and the Baltic region reveals some similarities with the complexes of the Baltic Shield.

2.2. Geology of the Lysan Complex Massifs

The Lysan alkaline–ultramafic complex is situated within the Sisim shear zone, located at the junction of the Precambrian Derba Block of the Sayano-Yenisei accretionary belt (as specified by [58]) and the Sisim-Kazyr zone of the Central Asian folded belt (Figure 2a). From an orographic perspective, the region is a confluence area for two mountain ranges in southern Siberia: the Western Sayan and the Eastern Sayan.

The Sisim Shear Zone comprises Bakhta Formation rocks within the Kuvai Group, which overlay the Neoproterozoic metacarbonate–terrigenous rocks of the Derba Group at a dipping unconformity. The rocks of the Bakhta Formation form an outcrop 4–5 km wide. These rocks are twisted in isoclinal folds which strike northwest.

The Bakhta Formation consists of basalts with interbeds of tuffs and tuff breccias, argillaceous shales, and tuff sandstones. The rocks are altered to chlorite and sericite schists, amphibole schists, amphibolites, and amphibole gneisses.

The intrusions of the Lysan Complex are distributed over an area of more than 150 km in a direction subparallel to the deep fault zone (Figure 2b). The original shape of the Massifs has not been preserved, existing in the present time as a plate- and lens-shaped body that extends towards the northwest and measures up to 5 km in length and 300 m in thickness. Mylonitization and cataclasis zones are present at the points of contact with the host rocks.

All massifs consist of ore-bearing olivinites, non-mineralized olivinites, serpentinites, kaersutite clinopyroxenites, and gabbroids (Figure 3). Olivinites and/or serpentinites are usually found in the centre of the massif. They are surrounded by clinopyroxenites and gabbro. The massifs also contain almost monomineral rocks composed mainly of albite, commonly called albitites [20]. Albitite veins or dykes typically occur at the interfaces between different rocks within the massif and occasionally along the boundaries between the massif and the host rock [20]. Thicknesses of the vein vary from 0.01 to 10 m, and vein lengths can be up to 1.5 km. Dykes of porphyritic picrites are present in some areas.

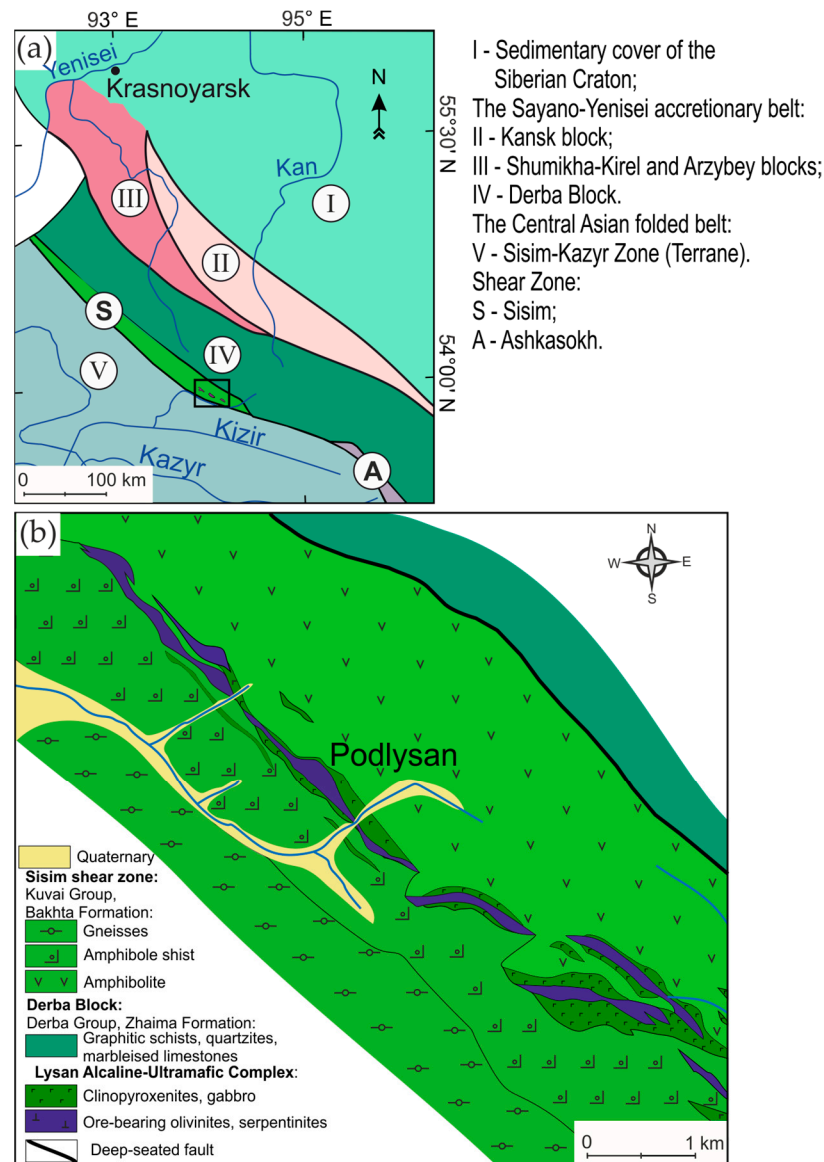


Figure 2. (a) Location of the massifs of the Lysan Complex (black rectangle) within the structures of South Siberia. The data used to create this map are sourced from [28,58]. (b) Simplified geological map of the area where the Lysan alkaline–ultramafic complex massifs are located, according to [59], with our modifications.

The largest Podlysan intrusive is located at the watershed of the Balakhtison River, a tributary of the Shinda River, and the Podlysan Creek, a right tributary of the Sisim River (Figure 3). It has a lenticular outline and a total length of 5 km, with a maximum thickness of up to 300 m. The outcrop area of olivinites and clinopyroxenites decreases significantly from northwest to southeast, while gabbro increases, as shown in Figure 3. There are similar changes in the proportions of olivinites, clinopyroxenites, and gabbros as the depth of the massif increases.

Albitite “dykes” and “veins” of varying thickness and lengths occur at the contact between clinopyroxenites and gabbro (Figure 3). The albitite contains carbonate veins and veinlets. The outcrops of these rocks show considerable weathering but the cores taken from boreholes are better preserved. Ore-bearing olivinites are composed of fine-grained idiomorphic olivine (FO_{80-82}) or pseudomorphs of serpentine on olivine (50–80 vol.%), titanomagnetite–ilmenite aggregates (15–45 vol.%), and minor allotriomorphic clinopyroxene ($WO_{50}En_{38}Fs_{11}$, 3.4–3.6 wt.% TiO_2). Hornblende commonly replaces clinopyrox-

ene. Kaersutite clinopyroxenites are medium-grained rocks consisting of clinopyroxene (55–45 vol.%), ferrokaersutite (35–54 vol.%), ilmenite (8–12 vol.%), and minor apatite and titanite. Ferrokaersutite (5.2–6.0 wt.% TiO_2 , 0.3–0.4 Mg#) occurs as oikocrysts containing clinopyroxene ($\text{Wo}_{44}\text{En}_{46}\text{Fs}_{10}$, 0.9 wt.% TiO_2), apatite, and ilmenite chadacrysts. Kaersutite gabbro exhibits banded textures. Banding is formed by an alternation of leucocratic and melanocratic layers. Gabbro comprises of clinopyroxene (6–57 vol.%), plagioclase (38–47 vol.%), ferrokaersutite (30–35 vol.%), ilmenite (1–4 vol.%), minor apatite, and titanite. Primary plagioclase (An_{50-60}) and clinopyroxene ($\text{Wo}_{43}\text{En}_{46}\text{Fs}_{11}$, 0.9 wt.% TiO_2) occur only in relicts and are replaced by albite and ferrohastingsite, respectively.

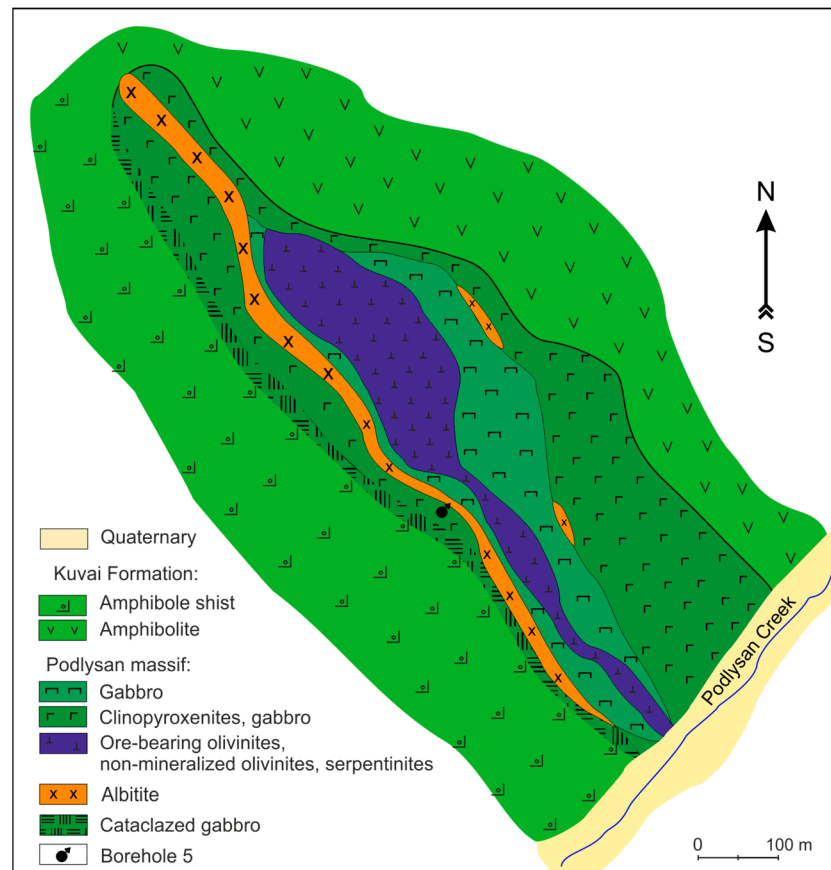


Figure 3. Simplified geological map of the northwestern part of the Podlysan Massif, according to [46], with our modifications.

The rock and mineral composition of the massifs in the Lysansky Complex exhibits significant similarity to the Lesnaya Varaka Massif in the Khabozerskaya Group located in the Kola Alkaline Province, Russia [50,60]. In this massif, as well as in the studied intrusions, ore-bearing olivinites, pyroxenites, and various rocks of the dyke complex are present [50,60,61]. The carbonatites of the Lesnaya Varaka Massif are of two types: dolomitic and apatite–dolomitic, with REE mineralization associated with the latter. The Lesnaya Varaka Massif is regarded as the most extensively eroded and deepest segment of the complex alkaline–ultramafic intrusion among the massifs in the Kola Alkaline Province [50,60].

3. Materials and Methods

The petrography and mineralogy of the rocks in the Lysan Complex massifs are described based on our collection of rock samples from outcrops and drill cores. The description is based on a collection of 55 rock samples. The mineralogy of the carbonate rocks and albitites in the Podlysan Massif has been documented based on a rock sample obtained from drill hole number 5 (Figure 3). Rocks and minerals were analysed at the Isotope Geo-

chemical Research Centre, Vinogradov Institute of Geochemistry, Siberian Branch, Russian Academy of Sciences [62]. The mineral composition was determined in situ in a polished section by scanning electron microscopy, energy dispersive spectrometry (SEM EDS), and electron probe microanalysis (EPMA). SEM EDS analysis was performed on a Tescan MIRA 3 LMH electron microscope (Tescan, Brno, Czech Republic) with an AztecLive Advanced Ultim Max 40 energy dispersive analysis system (Oxford Instruments Analytical Ltd., Abingdon, UK). Analyses were performed at an acceleration voltage of 20 kV, probe current of ~0.5 nA, and a spectrum accumulation time of 10–50 s. The results were checked against reference standards of simple compounds and metals for the majority of the elements. EPMA was performed using a JXA8200 Superprobe (JEOL Ltd., Tokyo, Japan) under the following conditions: acceleration voltage of 20 kV, a beam current of 20 nA, a beam diameter of 1 μm , and a counting time of 10 s for major elements and 20 s or 30 s for trace elements. The background counts were 5 s or 10 s long for major elements and 15 s long for trace elements. Matrix corrections and analysed element contents were calculated using the ZAF (atomic number, absorption, and fluorescence) approach applying the software for quantitative analysis for Superprobe JXA–8200 (V01.42© 2024–2007, JEOL Ltd., Tokyo, Japan). The standards used for major and minor components were: F-phlogopite (Si, Al, K, Mg and F); diopside (Ca); albite (Na); Mn-garnet rhodonite (Mn); pyrope (Fe); Sr-glass (Sr); ZrSiO₄ (Zr); BaSO₄ (Ba); Ti-glass (Ti); Y-phosphate (Y); Cl-apatite (Cl and P); PbS (Pb); Cs₂RECl₆ (Cs); La-phosphate (La); Ce-phosphate (Ce); Eu-phosphate (Eu); and pure Sc and Nb. Detection limits were (3σ , in wt.%): 0.07 for Na, 0.06 for Al, 0.1 for Si, 0.02 for Ca, 0.09 for F, 0.02 for K, 0.04 for Mg, 0.01 for Fe, 0.02 for Mn, 0.08 for Nb, 0.04 for Ti, 0.16 for Ta, 0.15 for Zr, 0.09 for Th, 0.08 for U, 0.27 for Sr, 0.14 for Pb, 0.06 for Ba, 0.08 for La, 0.14 for Ce, 0.11 for Pr, 0.1 for Nd, 0.06 for Sm, 0.11 for Gd, 0.05 for Dy, and 0.18 for Y. The calculation of mineral structural formulae was undertaken using the CALCMIN software [63].

4. Results

4.1. Petrography Carbonate Rocks and Albitite

The relationships between the leucocratic kaersutite gabbro, albitite, and carbonate veins in the core sample are shown in Figure 4a. The carbonate veins and veinlets have a pale primrose-yellow colour, which contrasts with the almost white albitite background and the dark grey-green kaersutite gabbro background. There are no sharp intrusive contacts between the gabbro and albitite. Instead, a gradual transition is observed, as shown by the colour gradation in Figure 4b, due to the gradual increase in carbonates and plagioclase in the gabbro towards the carbonate veins. Moreover, the textural appearance of albitite resembles brecciated gabbro that has been impregnated with silicate–carbonate aggregates.

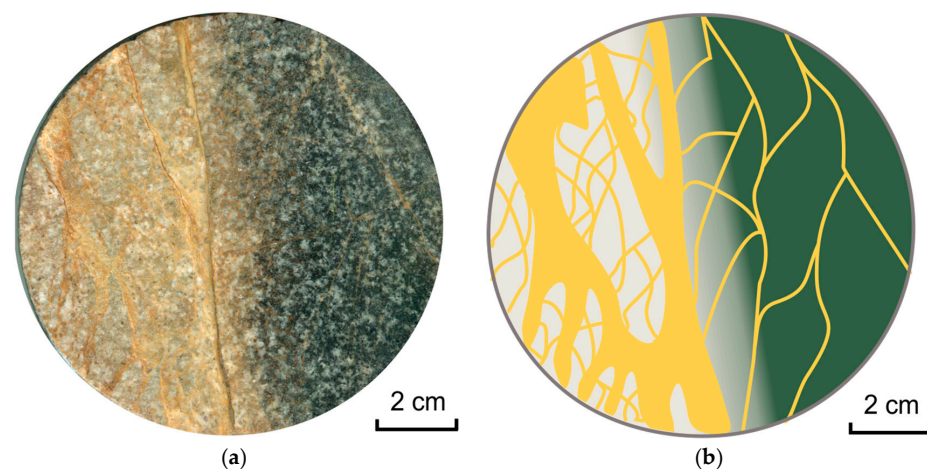


Figure 4. (a) Core sample cross-section. (b) The figure shows the relationship between kaersutite gabbro (Vizcaya-palm colour), albitite (elk-skin white colour), and carbonate rocks (pale primrose yellow colour) in a core section (left image).

The carbonate veins and veinlets are primarily located in the albite and vary in thickness from 0.1 to 10 mm. They are infrequent and thinner in the gabbro. Structurally, the large carbonate veins resemble flattened plates formed of transparent, pure euhedral and subhedral carbonate material. The centres of these veins consist of calcite, while the rims consist of aggregates of siderite, calcite, rare earth minerals, and albite (Figures 5a and 6). The small veins lack a zonal structure (Figure 5b).

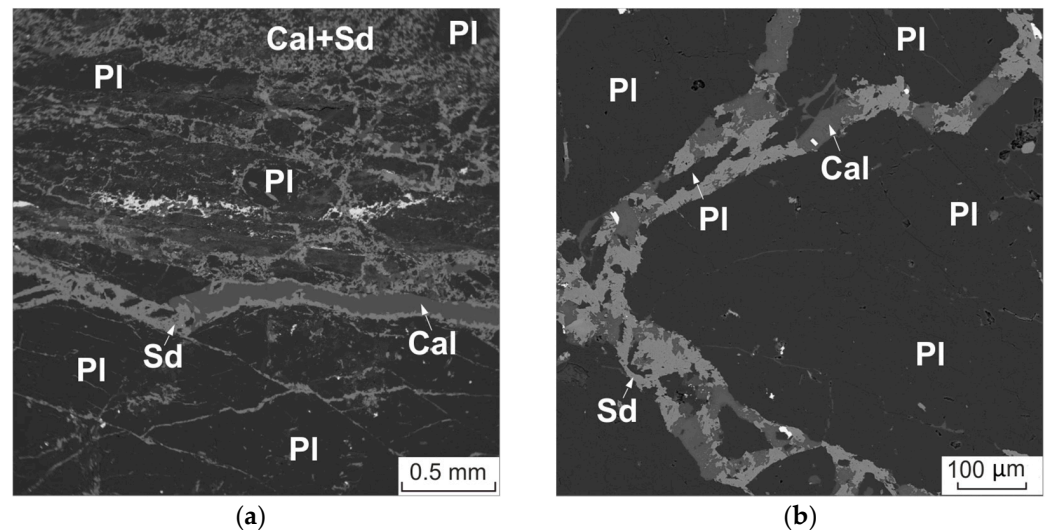


Figure 5. Calcite–siderite veinlets (light and dark grey) containing monazite (white) (a) and pyrite (white) (b) in an albite aggregate (black). Backscattered electron (BSE) image. Cal—calcite; Sd—siderite; Pl—plagioclase.

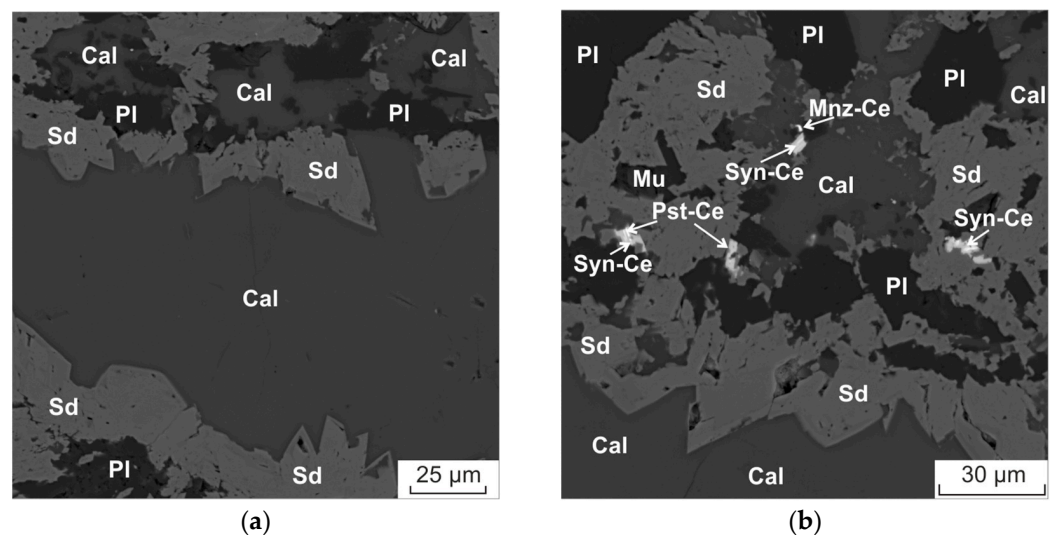


Figure 6. BSE image. (a) The central part of carbonate veins; (b) the rims of carbonate veins. Cal—calcite; Sd—siderite; Mu—white mica; Pl—plagioclase; Syn-Ce—synchysite-(Ce); Pst-Ce—parisite-(Ce); Mnz-Ce—monazite-(Ce).

There are three types of albites. The first type is monomineralic aggregates or large porphyroblasts (0.2–1 mm) localized between carbonate veins (Figure 7a). The second type consists of smaller sharp-angled porphyroclasts (50–100 µm) in the carbonate–silicate groundmass (Figure 7). The third type of grain is small, measuring less than 50 µm (Figure 6), and is often surrounded by a border of K-feldspar. This occurs in the carbonate–silicate groundmass.

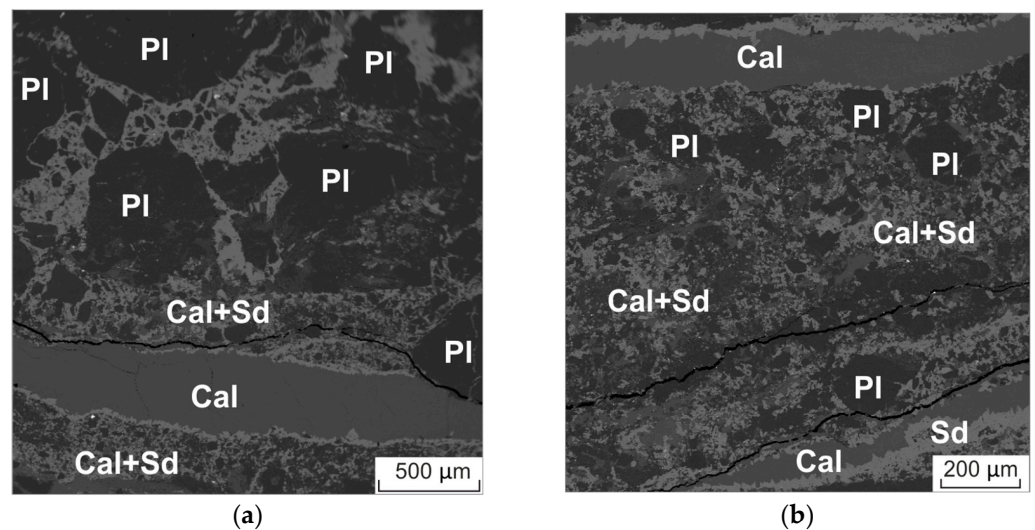


Figure 7. BSE image. (a) Calcite–siderite matrix between carbonate veins; (b) large albite grains in a rim of calcite–siderite clusters. Cal—calcite; Sd—siderite; Cal + Sd—carbonate–silicate matrix; Pl—plagioclase.

The groundmass is composed of calcite, siderite, white mica, K-feldspar, various accessory minerals, and sulphides. Determining the precise ratio of the main phases is a difficult task. However, it is worth noting that siderite is typically slightly more prevalent than calcite. Furthermore, white mica is a crucial phase.

Accessory minerals are apatite, rutile, zircon, monazite, REE fluorocarbonates, and an unidentified REE phase, listed in descending order of abundance.

Apatite crystals of varying sizes and forms are present. Small anhedral crystals (5–10 µm) are found within intergrowths alongside monazite in a siderite–calcite aggregate, whereas larger euhedral crystals (up to 0.1 mm) are present in a calcite–siderite–mica aggregate (see Figure S1). Rutile is observed as euhedral and subhedral crystals, ranging in size from 10 to 50 µm, forming intergrowths with apatite or monazite. Zircon grains are found in both the rims of large carbonate veins and in the carbonate–silicate groundmass. Most zircon grains are irregular in shape; sometimes, short prismatic or bipyramidal crystals are observed. The grain size ranges from 5–10 to 70–100 microns. Relics of baddeleyite are found in some crystals (Figure S2).

Monazite is typically found as small, individual grains measuring 5–10 µm in size, or as aggregates of subhedral and anhedral grains (Figure 8). Similar to zircon, it can also be found in the rims of large carbonate veins (Figure 6b) and in carbonate–silicate groundmass.

REE fluorocarbonates are bastnäsite-(Ce), parisite-(Ce), and synchysite-(Ce). Bastnäsite occurs as individual lamellar grains, with sizes ranging from 0.01 to 0.05 mm. Polycrystals with syntaxial intergrowths of parisite-(Ce) and synchysite-(Ce) were observed in siderite–calcite interstices (Figure 9).

The mineral phase containing rare earth elements and Ti, which remains unidentified, occurs in aggregates of rutile, siderite and mica as irregular grains measuring 10–20 microns. Pyrite and sphalerite occur as single crystals or as aggregates of subhedral or anhedral grains, occasionally forming sizable clusters ranging from 10–15 to 50–70 microns (Figure S3).

4.2. Mineral Chemistry

The albite porphyroblasts and porphyroclasts are similar in composition (An_{0-5}). Albite from the groundmass always contains K_2O , with a maximum amount of 2.2 wt%. The K-feldspar consistently contained Na_2O (0.4–1.9 wt%) and BaO (0.4–1.4 wt%). Additionally, Ce_2O_3 (1.4 wt%) was detected in one of the grains.

The composition of siderite, as shown in Table 1, exhibits varying contents of MnO, MgO, and CaO. The zonal crystals show an increase in CaO, MgO, and MnO concentrations from the core to the margin (1.5–2.7, 0–3.3, and 0.7–2.9 respectively).

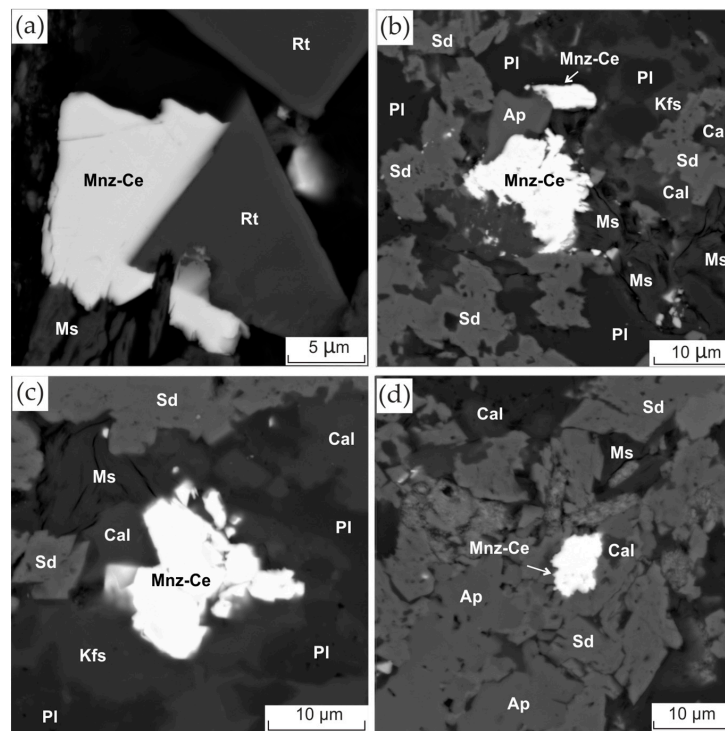


Figure 8. The morphology of monazite grains: in intergrowth with rutile (a); in aggregate with apatite, muscovite and plagioclase (b,c); in aggregate with calcite and siderite (d). Cal—calcite; Sd—siderite; Ms—white mica; Pl—plagioclase; Kfs—K-feldspar; Mnz-Ce—monazite-(Ce); Rt—rutile; Ap—apatite. BSE image.

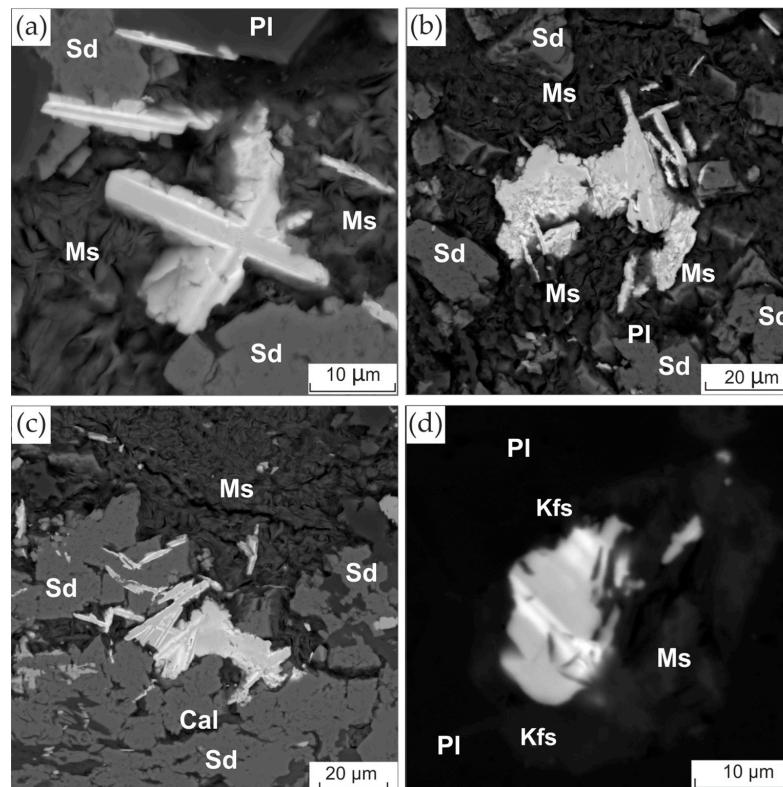


Figure 9. Syntaxial intergrowths of parisite-(Ce) and synchysite-(Ce) in muscovite aggregates (a,b); intergrown with calcite and siderite (c); in K-feldspar-muscovite aggregate (d). BSE image. Cal—calcite; Sd—siderite; Ms—white mica; Pl—plagioclase; Kfs—K-feldspar.

Table 1. Representative EPMA of siderite.

Oxide wt.%	7821	7821	7821-1	7821-1	7821-1	7821-1	7821-2	7821-2	7821-2	7821-2	7821-3	7821-3	7821-3	7821-3
FeO _t	52.03	51.16	51.97	51.92	59.04	46.02	52.90	52.75	52.92	56.08	54.67	45.80	52.28	54.27
MnO	3.91	1.38	0.97	3.14	0.71	0.78	0.42	2.31	0.64	1.04	3.13	0.68	0.87	1.47
MgO	3.12	6.00	5.64	3.50	0.00	3.61	4.43	4.62	4.48	1.84	2.86	7.46	6.06	3.44
CaO	2.80	2.92	3.05	2.86	1.68	10.07	3.54	1.78	2.99	2.41	1.37	7.26	2.49	2.06
Total	61.86	61.46	61.63	61.42	61.43	60.47	61.29	61.45	61.03	61.37	62.03	61.20	61.70	61.24
Structural formulae on the basis of 3 oxygens														
Fe	0.799	0.764	0.777	0.799	0.954	0.696	0.804	0.804	0.809	0.883	0.845	0.663	0.778	0.841
Mn	0.061	0.021	0.015	0.049	0.012	0.012	0.006	0.036	0.010	0.017	0.049	0.010	0.013	0.023
Mg	0.085	0.160	0.150	0.096	0.000	0.097	0.120	0.125	0.122	0.052	0.079	0.193	0.161	0.095
Ca	0.055	0.056	0.058	0.056	0.035	0.195	0.069	0.035	0.059	0.049	0.027	0.135	0.048	0.041
Cations	1.000	1.000	1.000	1.000	1.000	1.000	1.000	1.000	1.000	1.000	1.000	1.000	1.000	1.000

Calcite contains variable and appreciable amounts of FeO, MnO, and MgO, and only small amounts of SrO (0.9 wt.%) (Table 2, Figure 10). Calcite in the centre of the veins (Figure 5a) shows lower FeO and MnO abundances (1–1.3 wt% and <0.01–0.1 wt.%, respectively), compared to calcite from the groundmass (2.0–6.5 and 0.7–0.8 wt.%, respectively).

Table 2. Representative EPMA of calcite.

Oxide wt.%	7821	7821	7821	7821-1	7821-1	7821-1	7821-2	7821-2	7821-2	7821-3	7821-3	7821-3
FeO _t	4.04	1.76	0.40	2.00	2.33	3.83	1.62	1.88	2.74	2.70	1.34	1.69
MnO	2.35	1.85	0.77	0.81	0.34	0.90	0.62	0.95	0.18	0.53	0.94	0.00
MgO	0.28	0.18	0.00	0.14	0.36	0.26	0.18	0.18	0.15	0.18	0.00	0.18
CaO	49.39	51.43	54.19	51.64	52.34	49.16	51.35	52.05	53.13	50.46	52.95	52.83
SrO	0.86	0.25	0.19	0.56	0.26	0.26	0.82	0.47	0.27	0.46	0.20	0.40
Total	56.92	55.47	55.55	55.15	55.64	54.42	54.59	55.53	56.46	54.33	55.43	55.11
Structural formulae on the basis of 3 oxygens												
Fe	0.057	0.025	0.006	0.029	0.033	0.056	0.024	0.027	0.038	0.039	0.019	0.024
Mn	0.034	0.027	0.011	0.012	0.005	0.013	0.009	0.014	0.003	0.008	0.014	0.000
Mg	0.007	0.005	0.000	0.004	0.009	0.007	0.005	0.005	0.004	0.005	0.000	0.005
Ca	0.894	0.941	0.981	0.950	0.950	0.921	0.954	0.950	0.953	0.943	0.965	0.967
Sr	0.008	0.002	0.002	0.006	0.003	0.003	0.008	0.005	0.003	0.005	0.002	0.004
Cations	1.000	1.000	1.000	1.000	1.000	1.000	1.000	1.000	1.000	1.000	1.000	1.000

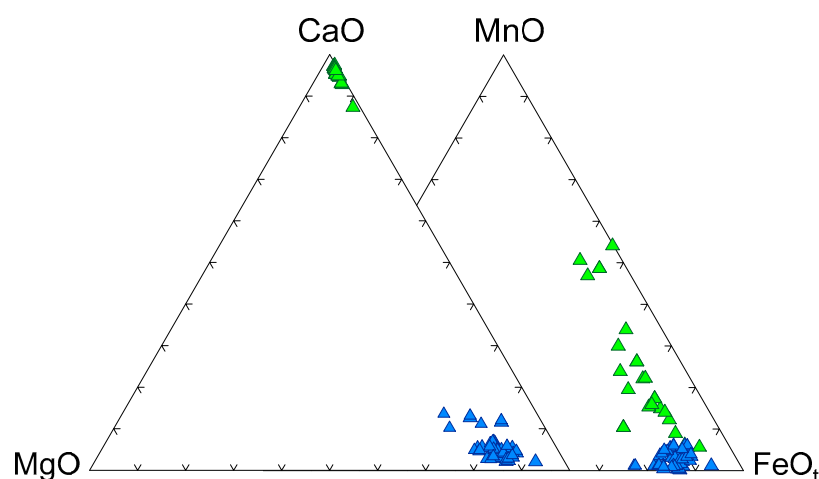


Figure 10. Composition of siderite (blue triangle) and calcite (green triangle).

The white mica is characterized by slightly higher SiO₂ (3.17–3.45 apfu), moderate FeO (0.14–0.28 apfu) and MgO (0.11–0.17 apfu), and high TiO₂ (up to 6.4 wt.%) contents (Figure S4, Table S1). The mica composition can be described as slightly phengitic muscovite.

Apatite is a fluorapatite with a homogeneous composition and a fluorine content of 4.1–4.8 wt.% (Table S2). The presence of Ce_2O_3 (0.3–0.9 wt.%) is noted in some grains. It is indicated that there are at least two generations of apatite. Rutile contains up to 2.5 wt.% Nb_2O_5 . Zircon contains ThO_2 (0.4–0.6 wt.%) and HfO_2 (0.9–1.5 wt.%).

The monazite composition is consistent with monazite-(Ce) (Table S3). Increased SiO_2 (3.0–5.9 wt.%) and ThO_2 (0.7–1.2 wt.%) were detected in some grains. Rare earth elements are typically found in the following proportions: $Ce > La > Nd > Pr > Sm > Gd$.

In the absence of a dedicated structural study of REE fluorocarbonates from carbonate veins within the Lysan Complex, mineral names have been assigned based on stoichiometric recalculations of analyses. On this basis, REE fluorocarbonates correspond in composition to bastnäsite-(Ce), parisite-(Ce), and synchysite-(Ce) (Table S4). Since the fluorine content was measured slightly lower than the theoretical amount, the deficiency was compensated for at this position by the calculated OH. REEs are typically found in the following ratios: $Ce > La > Nd > Pr > Y > Sm > Gd$. ThO_2 contents range from 0.8 to 5.1 wt.%.

The unidentified REE phases (Table S5) contain small amounts of SiO_2 (1.26–7.4 wt.%) and highly variable amounts of TiO_2 and CaO (6.5–25.6 and 87.8–13.2 wt.%, respectively). The main component of the composition of these phases is rare earth elements, the total amount of which is 35.7–50.3 wt.%. The rare earth elements in them occur in the same proportions as in REE fluorocarbonates: $Ce > La > Nd > Pr > Y > Sm > Gd$. ThO_2 (0.8–1.1 wt%) and fluorine (3.2–6.9 wt.%) are also present. According to the analysis results, the composition should contain carbonate or hydroxyl ions or both. These phases require further study. They were probably formed by the replacement of titanite or perovskite.

Pyrite is stoichiometric, without any additional elements. Some grains contain micro inclusions of galena and probably anglesite. Sphalerite typically contains Fe (4.1–5.9 wt.%) and occasionally Cu (up to 0.9 wt.%). The structural formula can be written as $Fe_{0.09}Cu_{0.01}Zn_{0.9}S$. Areas of atypical composition were detected in one of the grains, wt.-%: Fe—21.04; Cu—24.0; Zn—15.69; S—32.14.

5. Discussion

5.1. General Features of the Origin of Albitites and Carbonate Rocks of the Podlyansky Massif

5.1.1. Albitites

As mentioned earlier, it was previously believed that the albitite dykes in the Lysan Complex were of magmatic origin [26]. These dykes are found in cataclasis zones at contacts between petrographic rock differences within the massifs of the Lysan Complex or at contacts with host rocks. The examination of the relationship between albitite and leucocratic kaersutite gabbro in the drill core in this study did not reveal any evidence of intrusive contact between the rocks of the massif and albitite. The rock displays a gradual transition, which is attributed to an increase in carbonate and plagioclase content towards the carbonate veins. The textural and structural characteristics of albitite suggest that it was formed as a result of metasomatic alteration (finitization) of leucocratic gabbro in zones of intense development of tectonic fractures. The injection of metasomatizing fluids was preceded by the formation of apogabbroic cataclases. Where the fracturing of the gabbro is less pronounced, the compositional change is expressed only in plagioclase albitization. The sample shows observable effects of pervasive and vein finitization. However, the main mechanism for albitite formation was the infiltration of metasomatizing fluid. Similar transformations of metabasite substrates to albitite under the influence of ferricarbonate magma have been recorded in the Alpine Dyke Swarm, Westland, New Zealand [22,64], and the Kunene Intrusive Complex, NW Namibia [21].

Comparing the chemical composition of gabbro sampled at a distance from the albitite “dyke” with the composition of the albitite–carbonate mixture (see Table 3), it is clear that albitites are enriched in Na_2O and K_2O and depleted in FeO, CaO, and MgO. The albitite contains a large amount of metasomatically formed albite compared to the relatively small volume of the surrounding carbonate–silicate matrix. This suggests that the fluid responsible for metasomatism contained significant amounts of sodium prior to its loss during finitization.

Table 3. Bulck rock composition of the albitite (7821ac) and gabbro (68166), wt.%.

Sample #	SiO ₂	TiO ₂	Al ₂ O ₃	Fe ₂ O ₃	FeO	MnO	MgO	CaO	Na ₂ O	K ₂ O	P ₂ O ₅	CO ₂	H ₂ O	Total
7821ac	49.70	0.96	16.70	1.36	6.52	0.23	0.82	5.34	7.18	2.39	0.23	7.31	0.20	99.59
68166	48.80	1.58	15.57	3.43	8.41	0.13	5.54	11.70	1.89	0.42	0.27	0.51	1.14	99.01

5.1.2. Carbonate Rocks

The carbonate rocks found in the Podlysan Massif contain minerals such as calcite, siderite, apatite, Nb-bearing rutile, monazite-(Ce), REE fluorocarbonates, pyrite, and sphalerite, which are typomorphic to carbonatites (*sensu lato*). Most of the carbonatite complexes are typically associated with mica of the phlogopite series, but muscovite is a characteristic mineral of certain siderite carbonatites [11,14–16]. The muscovite composition in carbonate rocks of the Podlysan Massif is characterized by an increased concentration of TiO₂ and a slightly phengitic composition. Similar composition patterns have not been observed before in muscovite from known siderite carbonatites. However, some studies show that the high titanium content of phengite depends on the P-T conditions of its formation [65].

As mentioned earlier, carbonatites (*sensu lato*) are classified based on their mineralogy and texture as either primary, high-temperature magmatic rocks or low-temperature carbothermal remnants, known as carbothermalites [2,4]. This classification is non-genetic, as carbonatites can be formed through more than one route [2–6,9], just as carbothermalites can be derived from different parent magmas [2,4]. There are notable distinctions in the mineralogy, texture, and geochemical properties of intrusive carbonatites and carbothermalites. Carbothermalites are typically fine- to very fine-grained rocks with complex mineralogy and textures [4], which often makes them unsuitable for optical petrographic study due to their intricate nature. Intrusive carbonatites are sources of Nb, Ti, and P but not REE [2,4,7,9]. Carbothermal fluids were found to contain REE, Sr, and Ba but not Nb [2,4,7].

According to this classification [2,4], the carbonate rocks of the Podlysan Massif exhibit characteristics typical of carbothermalites. The minerals present are fine- and very fine-grained and form complex intergrowths (Figure 11). Common minerals identified include siderite, REE fluorocarbonates, zircon, and K-feldspar. Olivine, diopside, tetraferriphlogopite, magnetite, and perovskite are not present.

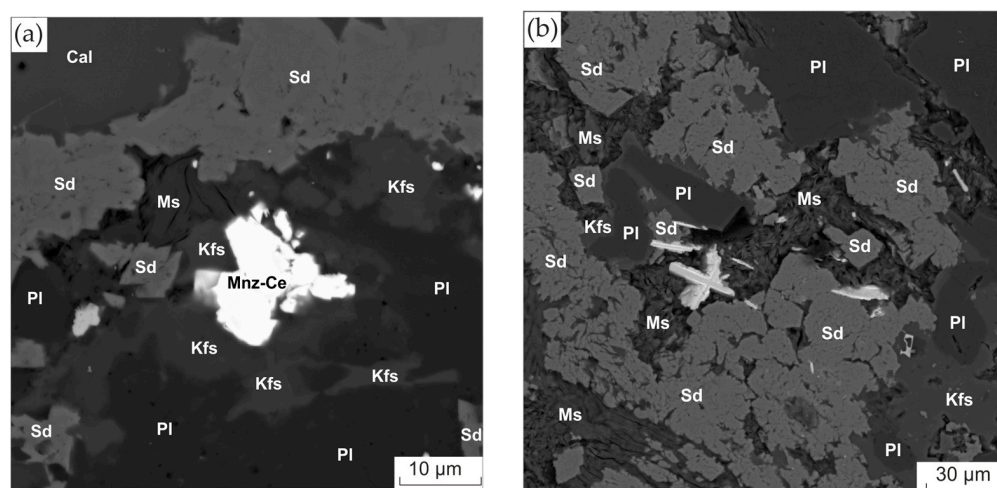


Figure 11. Relationships between rock-forming and accessory monazite-(Ce) (a) and REE-fluorocarbonates (b) in carbonate-silicate groundmass. BSE image. Cal—calcite; Sd—siderite; Ms—white mica; Pl—plagioclase; Kfs—K-feldspar.

The order of mineral crystallization in carbonate-silicate groundmass (Figure 11) can be inferred as follows: albite, K-feldspar, REE minerals, mica, siderite, and calcite. The syntaxial intergrowths of the Ca-REE fluorocarbonates are considered to be evidence of their

primary origin, with the intergrowths being related to changes in the chemical composition of the host fluid [66,67]. Based on the composition of calcite from carbonate veins, it appears that it crystallized after the carbonates from the groundmass. The formation of this most likely occurred during the hydrothermal stage.

Although it is considered difficult to find two identical carbonatites [5], the Haast River carbothermalites (or sideritic carbonatites according to [22,64]) found in the Alpine Dyke Swarm, Westland, New Zealand, exhibit similar textural features and mineral composition to those of the Podlysan Massif. Additionally, the composition of fenites resulting from the impact of fluid associated with these carbothermalites on metabasitic host rocks corresponds to almost monomineral albitite [22,64].

At this stage of the research, it is premature to determine the mechanisms responsible for the formation of carbonate rocks in the Podlysan Massif and their position in the formation of the dunite–pyroxenite–gabbro series.

However, when drawing an analogy with the Kola alkaline Province Complexes in Russia, it is important to note that there is some dependence between the occurrence of carbonatites, the petrographic composition of individual massifs, their degree of formation and the depth of denudation of intrusions [60]. Carbonatites (*sensu lato*) occur as individual, thin bodies within deeply eroded Massifs composed primarily of peridotites and pyroxenites. In shallower cross sections, carbonatite bodies become more numerous and unite into fields [60]. These fields are confined to zones of crushing or increased fracturing, as seen in the Vuorijärvi and Kovdor massifs [50,60]. Carbonatites are most prevalent in alkaline massifs, where early-phase peridotites occur as relict areas that have been strongly altered by alkaline metasomatism [60]. The Sallanlatvi and Ozernaya Varaka Massifs are good examples of this [13,60]. While the carbonatites of the Kovdor [68–71], Vuorijärvi [72], and Ozernaya Varaka [73] massifs have been extensively studied, the origin of the carbonate veins in the Lesnaya Varaka Massif remains unclear [60,74].

6. Conclusions

The Neoproterozoic Lysan alkaline–ultrabasic complex is an intricate object, requiring further geochemical, isotopic studies and petrological constructions. This study focused on the mineralogy of carbonate rocks and albitites, which are confined to fracture zones at the contacts between rock varieties within the massif and with the host rocks.

As a result, it has been established that:

1. The mineral composition of carbonate rocks corresponds to siderite carbonatites (*sensu stricto*). They contain calcite, siderite, phengitic muscovite, albite, K-feldspar, apatite, monazite-(Ce), Nb-bearing rutile, bastnäsite-(Ce), parisite-(Ce) and synchysite-(Ce), pyrite, and sphalerite.
2. Textural features suggest that they are carbothermalites formed from alkali-rich carbohydrothermal fluid.
3. Albitites were formed as a result of the phenitization of leucocratic gabbro by the infiltration of alkaline carbohydrothermal fluids in zones of intensive development of tectonic fractures.

The obtained results will provide a foundation for future studies focused on clarifying the origin of carbonate rocks in the Lysan Complex.

Supplementary Materials: The following supporting information can be downloaded at: <https://www.mdpi.com/article/10.3390/min14030290/s1>, Figure S1: Relationships between rock-forming and accessory minerals in a calcite–siderite matrix; Figure S2: Baddeleyite within zircon; Figure S3: Sulphide; Figure S4: Diagrams of the chemical composition of white micas; Figure S5: Unidentified REE phases in rutile–siderite–muscovite aggregate; Table S1: Representative composition of white mica; Table S2: Representative EPMA of apatite; Table S3: Representative EPMA of monazite; Table S4: Representative EPMA of REE fluorocarbonate; Table S5: Composition of unidentified REE phases.

Author Contributions: Conceptualization, T.B.K.; methodology, T.B.K. and A.S.M.; validation, Y.D.S.; investigation, A.S.M. and T.B.K.; resources, A.S.M.; writing—original draft preparation, T.B.K.;

writing—review and editing, T.B.K. and A.S.M. All authors have read and agreed to the published version of the manuscript.

Funding: This research was funded by the state order project number 0284-2021-0006.

Data Availability Statement: Data are contained within the article.

Acknowledgments: We are grateful to all anonymous reviewers for their careful reviews and constructive comments.

Conflicts of Interest: The authors declare no conflicts of interest.

References

1. Le Maitre, R.W.; Streckeisen, A.; Zanettin, B.; Le Bas, M.J.; Bonin, B.; Bateman, P.; Bellieni, G.; Dudek, A.; Efremova, S.; Keller, J.; et al. *Igneous Rocks: A Classification and Glossary of Terms—Recommendations of the International Union of Geological Sciences Subcommission on the Systematics of Igneous Rocks*, 2nd ed.; Le Maitre, R.W., Ed.; Cambridge University Press: Cambridge, UK, 2002; pp. 225–236.
2. Mitchell, R.H. Carbonatites and carbonatites and carbonatites. *Can. Mineral.* **2005**, *43*, 1833–1852. [[CrossRef](#)]
3. Jones, A.P.; Genge, M.; Carmody, L. Carbonate melts and carbonatites. *Rev. Mineral. Geochem.* **2013**, *75*, 289–322. [[CrossRef](#)]
4. Mitchell, R.H.; Gittins, J. Carbonatites and carbothermalites: A revised classification. *Lithos* **2022**, *430–431*, 106861. [[CrossRef](#)]
5. Kamenetsky, V.S.; Doroshevich, A.G.; Elliott, H.A.L.; Zaitsev, A.N. Carbonatites: Contrasting, Complex, and controversial. *Elements* **2021**, *17*, 307–314. [[CrossRef](#)]
6. Christy, A.; Pekov, I.; Krivovichev, S. The Distinctive mineralogy of carbonatites. *Elements* **2021**, *17*, 333–338. [[CrossRef](#)]
7. Chakhmouradian, A. High-field-strength elements in carbonatitic rocks: Geochemistry, crystal chemistry and significance for constraining the sources of carbonatites. *Chem. Geol.* **2006**, *235*, 138–160. [[CrossRef](#)]
8. Simandl, G.; Paradis, S. Carbonatites: Related ore deposits, resources, footprint, and exploration methods. *App. Earth Sci.* **2018**, *127*, 123–152. [[CrossRef](#)]
9. Anenburg, M.; Broom-Fendley, S.; Chen, W. Formation of rare earth deposits in carbonatites. *Elements* **2021**, *17*, 327–332. [[CrossRef](#)]
10. Loidolt, C.; Zimmermann, R.; Tusa, L.; Lorenz, S.; Ebert, D.; Gloaguen, R.; Broom-Fendley, S. New Insights into the Rare Earth Element Mineralization of the Storkwitz Carbonatite, Germany. *Can. Mineral.* **2023**, *60*, 913–932. [[CrossRef](#)]
11. Buckley, H.A.; Woolley, A.R. Carbonates of the magnesite-siderite series from four carbonatite Complexes. *Mineral. Mag.* **1990**, *54*, 413–418. [[CrossRef](#)]
12. Thompson, R.N.; Smith, P.M.; Gibson, S.A.; Matthey, D.P.; Dickin, A.P. Ankerite carbonatite from Swartbooisdrif, Namibia: The first evidence for magmatic ferrocyanatite. *Contrib. Miner. Petrol.* **2002**, *143*, 377–396. [[CrossRef](#)]
13. Zaitsev, A.N.; Sitnikova, M.A.; Subbotin, V.V.; Fernández-Suárez, J.; Jeffries, T.E. Sallanlatvi Complex—A rare example of magnesite and siderite carbonatites. In *Phoscorites and Carbonatites from Mantle to Mine: The Key Example of the Kola Alkaline Province*; Wall, F., Zaitsev, A.N., Eds.; Mineralogical Society of Great Britain and Ireland: London, UK, 2004; pp. 201–245.
14. Bolonin, A.V.; Nikiforov, A.V. Chemical composition of carbonatite minerals in Karasug deposit, Tuva. *Geol. Ore Dep.* **2004**, *46*, 372–386.
15. Giovannini, A.; Mitchell, R.; Bastos Neto, A.; Moura, C.; Pereira, V.; Porto, C. Mineralogy and geochemistry of the Morro dos Seis Lagos siderite carbonatite, Amazonas, Brazil. *Lithos* **2020**, *360–361*, 105433. [[CrossRef](#)]
16. Prokopyev, I.R.; Borisenko, A.S.; Borovikov, A.A.; Pavlova, G.G. Origin of REE-rich ferrocyanatites in southern Siberia (Russia): Implications based on melt and fluid inclusions. *Mineral. Petrol.* **2016**, *110*, 845–859. [[CrossRef](#)]
17. Morogan, V.; Woolley, A.R. Fenitization at the Alnö carbonatite Complex, Sweden; distribution, mineralogy and genesis. *Contrib. Miner. Petrol.* **1988**, *100*, 169–182. [[CrossRef](#)]
18. Morogan, V. Ijolite versus carbonatite as sources of fenitization. *Terra Nova* **1994**, *6*, 166–176. [[CrossRef](#)]
19. Le Bas, M.J. Fenites associated with carbonatites. *Can. Mineral.* **2008**, *46*, 915–932. [[CrossRef](#)]
20. Elliott, H.A.L.; Wall, F.; Chakhmouradian, A.R.; Siegfried, P.R.; Dahlgren, S.; Weatherley, S.; Deady, E. Fenites associated with carbonatite Complexes: A review. *Ore Geol. Rev.* **2018**, *93*, 38–59. [[CrossRef](#)]
21. Drüppel, K.; Hoefs, J.; Okrusch, M. Fenitizing processes induced by ferrocyanatite magmatism at Swartbooisdrif, NW Namibia. *J. Petrol.* **2005**, *46*, 377–406. [[CrossRef](#)]
22. Cooper, A.F.; Palin, J.M.; Collins, A.K. Fenitization of metabasic rocks by ferrocyanatites at Haast River, New Zealand. *Lithos* **2016**, *244*, 109–121. [[CrossRef](#)]
23. Brögger, W.C. *Die Eruptivgesteine des Kristianiagebietes: Das Fengebiet in Telemark, Norwegen*; Skrifter udgit av Videnskabselskabet i Kristiania, I, Matematisk-naturvidenskabelig klasse; In Kommission bei Jacob Dybwad: Kristiania, Norway, 1921; Volume 4, 408p.
24. Högbom, A.G. Über das Nephelinsyenitgebiet auf der Insel Alnö. *Geolog. Fören. Stockh. Förhandlingar* **1895**, *17*, 100–160. [[CrossRef](#)]
25. Hackman, V. Neue Mitteilungen über das Ijolithmassiv in Kuusamo. *Bull. Comm. Geolog. Finl.* **1899**, *11*, 1–52.
26. Glazunov, O.M. *Geochemistry and Petrology of the Gabbro-Pyroxenite Formation of the Eastern Sayan*; Vakhrushev, V.A., Ed.; Nauka: Novosibirsk, Russia, 1975; 216p. (In Russian)
27. Bognibov, V.I.; Izokh, A.E.; Polyakov, G.V.; Gibsher, A.S.; Mekhonoshin, A.S. Composition and geodynamic setting of formation of titanium-bearing ultramafic-mafic massifs in the Central Asian fold belt. *Rus. Geol. Geophys.* **2000**, *41*, 1083–1097.

28. Mekhonoshin, A.S.; Kolotilina, T.B.; Travin, A.V. Lysan alkaline-ultrabasic Complex (Eastern Sayan): Age and geodynamic consequences. *Geodyn. Tectonoph.* **2022**, *13*, 0651. (In Russian) [[CrossRef](#)]
29. Yarmolyuk, V.V.; Kovalenko, V.I.; Nikiforov, A.V.; Sal'nikova, E.B.; Kotov, A.B.; Vladyskin, N.V. Late Riphean rifting and breakup of Laurasia: Data on geochronological studies of ultramafic alkaline Complexes in the southern framing of the Siberian craton. *Dokl. Earth Sci.* **2005**, *404*, 1031–1036.
30. Ernst, R.E.; Hamilton, M.A.; Söderlund, U.; Hanes, J.A.; Gladkochub, D.P.; Okrugin, A.V.; Kolotilina, T.B.; Mekhonoshin, A.S.; Bleeker, W.; LeCheminant, A.N.; et al. Long-lived connection between southern Siberia and northern Laurentia in the Proterozoic. *Nat. Geosci.* **2016**, *9*, 464–469. [[CrossRef](#)]
31. Li, Z.X.; De Waele, B.; Pisarevsky, S.A.; Bogdanova, S.V.; Collins, A.S.; Davidson, A.; Ernst, R.E.; Fitzsimons, I.C.W.; Fuck, R.A.; Gladkochub, D.P.; et al. Assembly, configuration, and break-up history of Rodinia: A synthesis. *Precam. Res.* **2008**, *160*, 179–210. [[CrossRef](#)]
32. Zabrodin, V.Y.; Malyshev, A.A. New Complex of alkali-mafic rocks and carbonatites in Yenisei Ridge. *Dokl. Akad. Nauk SSSR* **1975**, *223*, 1223–1226. (In Russian)
33. Romanova, I.V.; Vernikovskaya, A.E.; Vernikovskiy, V.A.; Matushkin, N.Y.; Larionov, A.N. Neoproterozoic alkaline magmatism and associated igneous rocks in the western framing of the Siberian craton: Petrography, geochemistry, and geochronology. *Russ. Geol. Geophys.* **2012**, *53*, 1176–1196. [[CrossRef](#)]
34. Frolov, A.; Belov, S.V. Complex carbonate deposits of the Ziminsky ore district (East Sayan, Russia). *Geol. Ore Depos.* **1999**, *41*, 109–130. (In Russian)
35. Andreeva, I.A.; Kovalenko, V.I.; Nikiforov, A.V.; Kononkova, N.N. Compositions of magmas, formation conditions, and genesis of carbonate-bearing ijolites and carbonatites of the Belaya Zima alkaline carbonatite Complex, Eastern Sayan. *Petrology* **2007**, *15*, 551–574. [[CrossRef](#)]
36. Ashchepkov, I.; Zhmodik, S.; Belyanin, D.; Kiseleva, O.N.; Medvedev, N.; Travin, A.; Yudin, D.; Karmanov, N.S.; Downes, H. Aillikites and alkali ultramafic lamprophyres of the Beloziminsky alkaline ultrabasic-carbonatite massif: Possible origin and relations with ore deposits. *Minerals* **2020**, *10*, 404. [[CrossRef](#)]
37. Savelyeva, V.B.; Danilova, Y.V.; Letnikov, F.A.; Demonterova, E.I.; Yudin, D.S.; Bazarova, E.P.; Danilov, B.S.; Sharygin, I.S. Age and melt sources of ultramafic dykes and rocks of the Bolshetagninskii alkaline carbonatite massif (Urik-Iya graben, SW Margin of the Siberian Craton). *Dokl. Earth Sci.* **2022**, *505*, 452–458. [[CrossRef](#)]
38. Stifeeva, M.V.; Salnikova, E.B.; Savelyeva, V.B.; Kotov, A.B.; Danilova, Y.V.; Bazarova, E.P.; Danilov, B.S. Timing of carbonatite ultramafic Complexes of the Eastern Sayan alkaline Province, Siberia: U–Pb (ID–TIMS) Geochronology of Ca–Fe Garnets. *Minerals* **2023**, *13*, 1086. [[CrossRef](#)]
39. Konev, A.A. *Zhidoy Alkaline-Ultrabasic Pluton*; Nauka: Moscow, Russia, 1970; 84p. (In Russian)
40. Morikiyo, T.; Takano, K.; Miyazaki, T.; Kagami, H.; Vladyskin, N. Sr, Nd, C and O isotopic compositions of carbonatite and peralkaline silicate rocks from the Zhidoy Complex, Russia: Evidence for binary mixing, liquid immiscibility and a heterogeneous depleted mantle source region. *J. Miner. Petrol. Sci.* **2000**, *95*, 162–172. [[CrossRef](#)]
41. Vladyskin, N.V.; Sotnikova, I.A.; Alymova, N.V. Zhidoy Alkali-ultramafic rock and carbonatite massif: Geochemical features, its sources and ore-bearing. In *Alkaline Rocks, Kimberlites and Carbonatites: Geochemistry and Genesis*; Vladyskin, N.V., Ed.; Springer Nature: Cham, Switzerland, 2021; pp. 49–62. [[CrossRef](#)]
42. Doroshkevich, A.; Wall, F.; Ripp, G. Calcite-bearing dolomite carbonatite dykes from Veseloe, North Transbaikalia, Russia and possible Cr-rich mantle xenoliths. *Mineral. Petrol.* **2007**, *90*, 19–49. [[CrossRef](#)]
43. Doroshkevich, A.G.; Wall, F.; Ripp, G.S. Magmatic graphite in dolomite carbonatite at Pogranichnoe, North Transbaikalia, Russia. *Contrib. Mineral. Petrol.* **2007**, *153*, 339–353. [[CrossRef](#)]
44. Glagolev, A.A.; Korchagin, A.M.; Kharchenkov, A.G. *Arbarastakh and Inagli Alkaline-Ultrabasic Massifs*; Nauka: Moscow, Russia, 1974; 175p. (In Russian)
45. Prokopyev, I.R.; Doroshkevich, A.G.; Zhumadilova, D.V.; Starikova, A.E.; Nugumanova Ya, N.; Vladyskin, N.V. Petrogenesis of Zr–Nb (REE) carbonatites and phoscorites from the Arbarastakh Complex (Aldan Shield, Russia): Mineralogy and inclusion data. *Ore Geol. Rev.* **2021**, *131*, 104042. [[CrossRef](#)]
46. Kruk, M.N.; Doroshkevich, A.G.; Prokopyev, I.R.; Izbrodin, I.A. Mineralogy of phoscorites of the Arbarastakh Complex (Republic of Sakha, Yakutia, Russia). *Minerals* **2021**, *11*, 556. [[CrossRef](#)]
47. Doroshkevich, A.; Prokopyev, I.; Kruk, M.; Sharygin, V.; Izbrodin, I.; Starikova, A.; Ponomarchuk, A.; Izokh, A.; Nugumanova, Y. Age and petrogenesis of ultramafic lamprophyres of the Arbarastakh alkaline-carbonatite Complex, Aldan-Stanovoy Shield, South of Siberian craton (Russia): Evidence for ultramafic lamprophyre-carbonatite link. *J. Petrol.* **2022**, *63*, 9. [[CrossRef](#)]
48. Shadenkov, E.M. New data on geology of the Ingili intrusion. *Geol. Pac. Ocean* **1994**, *6*, 1061–1073.
49. Buslov, M.M. Terrain tectonics of the Central Asian folded belt. *Geodyn. Tectonoph.* **2014**, *5*, 641–665. [[CrossRef](#)]
50. Kogarko, L.N.; Kononova, V.A.; Orlova, M.R.; Woolley, A.R. *Alkaline Rocks and Carbonatites of the World. Part 2. Former USSR*; Chapman and Hall: London, UK, 1995; 226p. [[CrossRef](#)]
51. Kinnaird, J.A.; Bowden, P. Magmatism and mineralization associated with Phanerozoic Anorogenic Plutonic Complexes of the African Plate. In *Magmatism in Extensional Structural Settings: The Phanerozoic African Plate*; Kampunzu, A., Lubala, R.T., Eds.; Springer: Berlin, Germany, 1991; pp. 410–485.
52. Ernst, R.E.; Bell, K. Large igneous provinces (LIPs) and carbonatites. *Mineral. Petrol.* **2010**, *98*, 55–76. [[CrossRef](#)]

53. Woolley, A.R.; Kjarsgaard, B.A. Carbonatite occurrences of the world: Map and database. *Geol. Surv. Can.* **2008**, 5796.
54. Tappe, S.; Foley, S.F.; Kjarsgaard, B.A.; Romer, R.L.; Heaman, L.M.; Stracke, A.; Jenner, G.A. Between carbonatite and lamproite—Diamondiferous Torngat ultramafic lampropyres formed by carbonate-fluxed melting of cratonic MARID-type metasomes. *Geochim. Cosmochim. Acta* **2008**, *72*, 3258–3286. [[CrossRef](#)]
55. Tappe, S.; Foley, S.F.; Jenner, G.A.; Heaman, L.M.; Kjarsgaard, B.A.; Romer, R.L.; Stracke, A.; Joyce, N.; Hoefs, J. Genesis of ultramafic lamprophyres and carbonatites at Aillik Bay, Labrador: A consequence of incipient lithospheric thinning beneath the North Atlantic craton. *J. Petrol.* **2006**, *47*, 261–315. [[CrossRef](#)]
56. Kresten, P.; Printzlau, I.; Rex, D.; Vartiainen, H.; Woolley, A. New ages of carbonatitic and alkaline ultramafic rocks from Sweden and Finland. *GFF* **1977**, *99*, 62–65. [[CrossRef](#)]
57. Kresten, P.; Troll, V.R. *The Alnö Carbonatite Complex, Central Sweden*; Springer Nature: Cham, Switzerland, 2018; 222p.
58. Nozhkin, A.D.; Turkina, O.M.; Dmitrieva, N.V.; Travin, A.V.; Likhanov, I.I. Metacarbonate-terrigenous Complex of the Derba Block (East Sayan): Petrogeochemical and isotope parameters, Metamorphism, and Time of Formation. *Russ. Geol. Geophys.* **2018**, *59*, 652–672. [[CrossRef](#)]
59. Glazunov, O.M.; Mekhonoshin, A.S.; Zakharov, M.N. *Geochemistry of Iron Group Elements in the Endogenous Process*; Seminsky, J.V., Ed.; Nauka Siberian Branch: Novosibirsk, Russia, 1985; 200p. (In Russian)
60. Kukhareno, A.A.; Orlova, M.P.; Bulakh, A.G.; Bagdasarov, E.A.; Rimskaya-Korsakova, O.M.; Nefedov, E.I.; Ilyinsky, G.A.; Sergeev, A.S.; Abakumova, N.B. *Caledonian Complex of Ultrabasic, Alkaline Rocks and Carbonatites of the Kola Peninsula and North Karelia*; Kukhareno, A.A., Ed.; Nedra: Moscow, Russia, 1965; 772p. (In Russian)
61. Barkov, A.Y.; Tarkian, M.; Laajoki, K.V.O.; Gehör, S.A. Primary platinum-bearing copper from the Lesnaya Varaka ultramafic alkaline Complex, Kola Peninsula, northwestern Russia. *Mineral. Petrol.* **1998**, *62*, 61–72. [[CrossRef](#)]
62. Skuzovatov, S.Y.; Belozero, O.Y.; Vasil'eva, I.E.; Zarubina, O.V.; Kaneva, E.V.; Sokolnikova, Y.V.; Chubarov, V.M.; Shabanova, E.V. Centre of isotopic and geochemical research (IGC SB RAS): Current state of micro- and macroanalysis. *Geodyn. Tectonophys.* **2022**, *13*, 0585. (In Russian) [[CrossRef](#)]
63. Brandelik, A. CALCMIN—An EXCEL™ Visual Basic application for calculating mineral structural formulae from electron microprobe analyses. *Comput. Geosci.* **2009**, *35*, 1540–1551. [[CrossRef](#)]
64. Cooper, A.F.; Paterson, L.A. Carbonatites from a lamprophyric dyke-swarm, South Westland, New Zealand. *Can. Mineral.* **2008**, *46*, 753–777. [[CrossRef](#)]
65. Auzanneau, E.; Schmidt, M.W.; Vielzeuf, D.; Connolly, J.A.D. Titanium in phengite: A geobarometer for high temperature eclogites. *Contrib. Mineral. Petrol.* **2010**, *159*, 1–24. [[CrossRef](#)]
66. Ni, Y.; Huges, J.M.; Mariano, A.N. The atomic arrangement of bastnäsite-(Ce), Ce(CO₃)F, and structural elements of synchysite-(Ce), röntgenite-(Ce), and parisite-(Ce). *Am. Mineral.* **1993**, *78*, 415–418.
67. Zaitsev, A.N.; Wall, F.; Le Bas, M.J. REE-Sr-Ba minerals from the Khibina carbonatites Kola Peninsula, Russia: Their mineralogy, paragenesis and evolution. *Mineral. Mag.* **1998**, *62*, 225–250. [[CrossRef](#)]
68. Ivanyuk, G.Y.; Kalashnikov, A.O.; Pakhomovsky, Y.A.; Bazai, A.V.; Goryainov, P.M.; Mikhailova, J.A.; Yakovenchuk, V.N.; Konopleva, N.G. Subsolidus Evolution of the magnetite-spinel-ulvöspinel solid solutions in the Kovdor phoscorite-carbonatite Complex, NW Russia. *Minerals* **2017**, *7*, 215. [[CrossRef](#)]
69. Mikhailova, J.A.; Ivanyuk, G.Y.; Kalashnikov, A.O.; Pakhomovsky, Y.A.; Bazai, A.V.; Panikorovskii, T.L.; Yakovenchuk, V.N.; Konopleva, N.G.; Goryainov, P.M. Three-D mineralogical mapping of the Kovdor phoscorite-carbonatite Complex, NW Russia: I. Forsterite. *Minerals* **2018**, *8*, 260. [[CrossRef](#)]
70. Ivanyuk, G.Y.; Pakhomovsky, Y.A.; Panikorovskii, T.L.; Mikhailova, J.A.; Kalashnikov, A.O.; Bazai, A.V.; Yakovenchuk, V.N.; Konopleva, N.G.; Goryainov, P.M. Three-D mineralogical mapping of the Kovdor phoscorite-carbonatite Complex, NW Russia: II. Sulfides. *Minerals* **2018**, *8*, 292. [[CrossRef](#)]
71. Ivanyuk, G.Y.; Konopleva, N.G.; Yakovenchuk, V.N.; Pakhomovsky, Y.A.; Panikorovskii, T.L.; Kalashnikov, A.O.; Bocharov, V.N.; Bazai, A.A.; Mikhailova, J.A.; Goryainov, P.M. Three-D mineralogical mapping of the Kovdor phoscorite-carbonatite Complex, NW Russia: III. Pyrochlore supergroup minerals. *Minerals* **2018**, *8*, 277. [[CrossRef](#)]
72. Brassinnes, S.; DemaiFFE, D.; Balaganskaya, E.; Downes, H. New mineralogical and geochemical data on the Vuorijarvi ultramafic, alkaline and carbonatitic Complex (Kola Region, NW Russia). *Period. Mineral.* **2003**, *72*, 79–86.
73. Reguir, E.P.; Chakhmouradian, A.R.; Pisiak, L.; Halden, N.M.; Yang, P.; Xu, C.; Kynicky, J.; Couëslan, C.G. Trace-element composition and zoning in clinopyroxene- and amphibole-group minerals: Implications for element partitioning and evolution of carbonatites. *Lithos* **2012**, *128–131*, 27–45. [[CrossRef](#)]
74. Chakhmouradian, A.R.; Mitchell, R.H. Lueshite, pyrochlore and monazite-(Ce) from apatite-dolomite carbonatite, Lesnaya Varaka Complex, Kola Peninsula, Russia. *Mineral. Mag.* **1998**, *62*, 769–782. [[CrossRef](#)]

Disclaimer/Publisher's Note: The statements, opinions and data contained in all publications are solely those of the individual author(s) and contributor(s) and not of MDPI and/or the editor(s). MDPI and/or the editor(s) disclaim responsibility for any injury to people or property resulting from any ideas, methods, instructions or products referred to in the content.